A STUDY ON THE MIXED CONVECTION BOUNDARY LAYER FLOW AND HEAT TRANSFER OVER A VERTICAL SLENDER CYLINDER

by

Rahmat ELLAHI [a,b*], Arshad RIAZ [b], Saeid ABBASBANDY [c], Tasawar HAYAT [d,e], and Kambiz VAFAI [a]

[a] Department of Mechanical Engineering, Bourns Hall, University of California, Riverside, Cal., USA
[b] Department of Mathematics, Faculty of Basic and Applied Science, International Islamic University, Islamabad, Pakistan
[c] Department of Mathematics, Science and Research Branch, Islamic Azad University, Tehran, Iran
[d] Department of Mathematics, Quaid-i-Azam University, Islamabad, Pakistan
[e] Department of Mathematics, Faculty of Science, King Abdulaziz University, Jeddah, Saudi Arabia

Original scientific paper
DOI: 10.2298/TSCI110923097E

In this investigation, the series solutions of mixed convection boundary layer flow over a vertical permeable cylinder are constructed. Two types of series as well numerical solutions are presented by choosing exponential and rational bases. The resulting differential system are solved by employing homotopy analysis method and Pade technique which have been proven to be successful in tackling non-linear problems. We offer various verifications of the solutions by comparing to existing, documented results and also mathematically, through reduction of sundry parameters. The convergence of the series solutions have been discussed explicitly. Comparison with existing results reveal that the series solutions are not only valid for large (aiding flow) but also for small values (opposing flow) of λ and the dual solutions do not obtain in both cases.

Key words: *mixed convection, series solutions, homotopy analysis method, Pade technique, porous cylinder, steady flow*

Introduction

The mixed convection flows under boundary layer analysis are of fundamental theoretical and practical interest. Heat exchangers, electric transformers, refrigeration coils, solar collectors, study of movement of natural gas, oil, water through oil reservoirs and nuclear reactors are few examples in this direction. The flows of non-Newtonian fluids through a porous medium[1-6] are also quite prevalent in nature. Examples of these applications are filtration processes, biomechanics, packed bed, ceramic geothermal engineering, insulation systems, ceramic processing, chromatography, and geophysical phenomena. Over the last several decades a large number of research work related to the mixed convection flow of a viscous and incompressible fluid over a vertical flat plate was conducted by a number of investigators. For instance, a critical review of mixed convection flows has been presented by Pop and Ingham [7].

* Corresponding author; e-mail: rellahi@engr.ucr.edu

Mahmood and Merkin [8] have presented dual similarity solutions for the axisymmetric mixed convection boundary layer flow along a vertical cylinder in the case of opposing directions only. Later on Ridha [9] has reported that when the buoyancy force acts in the direction of flow then the dual solutions for aiding flow also exist. Ishak *et al.* [10] have also reported a numerical simulation by Keller-box method for boundary layer flow and heat transfer over a vertical slender cylinder. In this study, the authors concluded that for aiding/assisting flow dual solutions exist but for opposing flow there are either dual solutions, unique solutions or no solution exist.

The purpose of the present investigation is to revisit the problem formulated in references [7-10] for the analytic solutions. The main stream velocity and wall surface temperature depend upon the axial distance along the cylinder surface. The homotopy analysis method (HAM) [11] has been applied to obtain series solutions of velocity and temperature fields by making choices of two base functions. Convergence of the obtained series solutions is taken care properly. Furthermore, the skin friction and Nusselt number are analyzed. Comparison with the previous relevant studies is made. To the best of our knowledge, the series solutions for this particular model have not been presented in the past. It is worth mentioning that in both cases, the dual solutions do not exist, therefore, the comparison with existing results reveal that our series solutions are valid for $\lambda > 0$ (heated cylinder) and for $\lambda < 0$ (cooled cylinder) as well. It is shown that like several existing studies [12-18], the HAM in the present paper is accepted as an elegant tool for effective solutions for a number of complicated fluid problems.

Problem formulation

Here, we analyze the convection flow and heat transfer characteristic along a vertical permeable slender cylinder with radius a. We choose the cylindrical co-ordinates (x, r) such that x- and r-axes are along the cylinder surface (vertically) and radial directions, respectively. Symmetric nature of the flow is assumed with respect to the transverse co-ordinate. Furthermore, cylinder is kept in an incompressible viscous fluid of uniform ambient temperature T_∞ and constant density ρ_∞. Using continuity, momentum, and energy equations, one obtains the following boundary layer equations [19, 20]:

$$\frac{\partial}{\partial x}(ru) + \frac{\partial}{\partial r}(rw) = 0 \tag{1}$$

$$u\frac{\partial u}{\partial x} + w\frac{\partial u}{\partial r} = U\frac{\mathrm{d}U}{\mathrm{d}x} + \nu\left(\frac{\partial^2 u}{\partial r^2} + \frac{1}{r}\frac{\partial u}{\partial r}\right) + g\beta(T - T_\infty) \tag{2}$$

$$u\frac{\partial T}{\partial x} + w\frac{\partial T}{\partial r} = \alpha\left(\frac{\partial^2 T}{\partial r^2} + \frac{1}{r}\frac{\partial T}{\partial r}\right) \tag{3}$$

In the equations, u and w indicate the velocity components, $U(x)$ – the mainstream velocity, T – the fluid temperature, g – the gravitational acceleration, α – the thermal diffusivity, β – the thermal expansion coefficient, and ν – the kinematic viscosity. The subjected boundary conditions are [10]:

$$u = 0, \quad w = V, \quad T = T_w(x), \quad \text{at} \quad r = a \tag{4}$$

$$u \to U(x), \quad T \to T_\infty, \quad \text{as} \quad r \to \infty \tag{5}$$

where $V(>0)$ and $V(<0)$ correspond to the injection and suction velocities, respectively. Further, $U(x)$ and temperature of the cylinder surface $T_w(x)$ are:

$$U(x) = U_\infty\left(\frac{x}{\ell}\right), \quad T_w(x) = T_\infty + \Delta T\left(\frac{x}{\ell}\right) \tag{6}$$

in which ℓ denotes characteristic length and ΔT is the characteristic temperature. Note that $\Delta T > 0$ corresponds to a heated surface and $\Delta T < 0$ for a cooled surface.

Defining

$$\eta = \frac{r^2 - a^2}{2a}\left(\frac{U}{\nu x}\right)^{0.5}, \quad \psi = (U\nu x)^{0.5} a f(\eta), \quad \theta(\eta) = \frac{T - T_\infty}{T_w - T_\infty} \tag{7}$$

$$u = Uf'(\eta), \quad w = -\frac{a}{r}\left(\frac{\nu U_\infty}{\ell}\right)^{0.5} f(\eta) \tag{8}$$

where the stream function ψ can be defined by $u = r^{-1}\partial\psi/\partial r$ and $w = -r^{-1}\partial\psi/\partial x$. Moreover prime denotes differentiation with respect to η.

Invoking eqs. (7) and (8), eq. (1) is identically satisfied, and eqs. (2) and (3) yield:

$$(1 + 2\gamma\eta) f'''(\eta) + 2\gamma f''(\eta) + f(\eta) f''(\eta) + 1 - [f'^2(\eta) + \lambda\theta(\eta)] = 0 \tag{9}$$

$$(1 + 2\gamma\eta)\theta''(\eta) + 2\gamma\theta'(\eta) + \Pr[f(\eta)\theta'(\eta) - f'(\eta)\theta(\eta)] = 0 \tag{10}$$

and the curvature parameter γ and V are:

$$\gamma = \left(\frac{\nu\ell}{U_\infty a^2}\right)^{0.5}, \quad V = -\frac{a}{r}\left(\frac{\nu U_\infty}{\ell}\right)^{0.5} f_0$$

where $f_0 = f(0)$. It is noted that $f_0 < 0$ is for mass injection and $f_0 > 0$ is for mass suction. The buoyancy or mixed convection parameter λ is:

$$\lambda = \frac{g\beta\ell\Delta T}{U_\infty^2}$$

Here $\lambda > 0$ and $\lambda < 0$ are for aiding flow (heated cylinder) and for opposing flow (cooled cylinder), respectively. For $\lambda = 0$, one has pure forced convection flow without buoyancy force.

The boundary conditions (4) and (5) reduce in the form:

$$f(0) = f_0, \quad f'(0) = 0, \quad f'(\infty) = 1, \quad \theta(0) = 1, \quad \theta(\infty) = 0 \tag{11}$$

Now the skin friction coefficient (C_f) and the local Nusselt number (Nu_x) are:

$$C_f = \frac{\tau_w}{\frac{\rho U^2}{2}}, \quad Nu_x = \frac{x q_w}{k(T_w - T_\infty)} \tag{12}$$

where $\rho = \rho_\infty[1 - \beta(T - T_\infty)]$ and the skin friction τ_w and the heat transfer from the plate q_w can be written as:

$$\tau_w = \mu\left(\frac{\partial u}{\partial r}\right)_{r=a}, \quad q_w = -k\left(\frac{\partial T}{\partial r}\right)_{r=a}$$

in which μ and k are the dynamic viscosity and thermal conductivity, respectively. Making use by eq. (7) one obtains:

$$\frac{1}{2} C_f (Re_x)^{0.5} = f''(0), \quad \frac{Nu_x}{(Re_x)^{0.5}} = -\theta'(0) \tag{13}$$

Expression $Re_x = Ux/\nu$ denotes the local Reynold number [10].

Solution of the problem

Here we offer two types of series solutions by choosing exponential and rational bases.

Exponential bases

According to eqs. (9) and (10) and the boundary conditions (11), we write the solution in the form:

$$f(\eta) = a_0 + \eta + \sum_{m=1}^{+\infty} \sum_{q=0}^{\infty} a_{q,m} \eta^q \mathrm{e}^{-m\zeta\eta} \tag{14}$$

$$\theta(\eta) = \sum_{m=1}^{+\infty} \sum_{q=0}^{\infty} b_{q,m} \eta^q \mathrm{e}^{-m\zeta\eta} \tag{15}$$

where a_0, $a_{q,m}$, and $b_{q,m}$ are coefficients to be determined and ζ is a spatial-scale parameter. By rule of solution expression denoted by eqs. (14) and (15) and the boundary conditions (11), it is natural to choose:

$$f_0(\eta) = f_0 + \tau - \frac{1 - \exp(-\zeta\tau)}{\zeta} \tag{16}$$

$$\theta_0(\eta) = \mathrm{e}^{-\zeta\eta} \tag{17}$$

as the initial approximation to $f(\eta)$ and $\theta(\eta)$, respectively. We use the method of higher order differential mapping, [21] to choose the auxiliary linear operators L_1 and L_2 by:

$$\mathrm{L}_1[\phi(\eta,\zeta;p)] = \left(\frac{\partial^3}{\partial\eta^3} + \zeta\frac{\partial^2}{\partial\eta^2}\right)\phi(\eta,\zeta;p) \tag{18}$$

$$\mathrm{L}_2[\psi(\eta,\zeta;p)] = \left(\frac{\partial^2}{\partial\eta^2} + \zeta\frac{\partial^2}{\partial\eta}\right)\psi(\eta,\zeta;p) \tag{19}$$

which satisfy the properties:

$$\mathrm{L}_1[C_1 + C_2\eta + C_3\mathrm{e}^{-\zeta\eta}] = 0, \quad \mathrm{L}_2[C_4 + C_5\mathrm{e}^{-\zeta\eta}] = 0 \tag{20}$$

where C_i, $i = 1, 2, \ldots$, are constants. This choice of L_1 and L_2 is motivated by eqs. (14) and (15), respectively, and from boundary conditions (11), we have $C_2 = C_4 = 0$.

From (9) and (10) we define non-linear operators as:

$$\mathrm{N}_1[\phi(\eta,\zeta;p),\psi(\eta,\zeta;p)] = (1+2\gamma\eta)\frac{\partial^3}{\partial\eta^2} + 2\gamma\frac{\partial^2\phi}{\partial\eta^2} + \phi\frac{\partial^2\phi}{\partial\eta^2} + 1 - \left(\frac{\partial\phi}{\partial\eta}\right)^2 + \lambda\psi \tag{21}$$

$$\mathrm{N}_2[\phi(\eta,\zeta;p),\psi(\eta,\zeta;p)] = (1+2\gamma\eta)\frac{\partial^2\psi}{\partial\eta^2} + 2\gamma\frac{\partial\psi}{\partial\eta} + \mathrm{Pr}\left(\phi\frac{\partial\psi}{\partial\eta} - \psi\frac{\partial\phi}{\partial\eta}\right) \tag{22}$$

and then construct the homotopy:

$$\mathrm{H}_1[\phi(\eta,\zeta;p),\psi(\eta,\zeta;p)] = (1-p)\mathrm{L}_1[\phi - f_0(\eta)] - \hbar_1 p\mathrm{H}_1(\eta)\mathrm{N}_1[\phi,\psi] \tag{23}$$

$$\mathrm{H}_2[\phi(\eta,\zeta;p),\psi(\eta,\zeta;p)] = (1-p)\mathrm{L}_2[\psi - \theta_0(\eta)] - \hbar_2 p\mathrm{H}_2(\eta)\mathrm{N}_2[\phi,\psi] \tag{24}$$

where $\hbar_1 \neq 0$ and $\hbar_2 \neq 0$ are the convergence-control parameters [22], $\mathrm{H}_1(\eta)$ and $\mathrm{H}_2(\eta)$ are auxiliary functions. Setting $\mathrm{H}_i[\phi(\eta,\zeta;p), \psi(\eta,\zeta;p)] = 0$, for $i = 1, 2$, we have the following zero-order deformation problems:

$$(1-p)\mathrm{L}_1[\phi - f_0(\eta)] = \hbar_1 p \mathrm{H}_1(\eta)\mathrm{N}_1[\phi,\psi] \tag{25}$$

$$(1-p)\mathrm{L}_2[\phi - f_0(\eta)] = \hbar_2 p \mathrm{H}_2(\eta)\mathrm{N}_2[\phi,\psi] \tag{26}$$

subject to conditions:

$$\phi(0,\zeta;p) = f_0, \quad \left.\frac{\partial\phi(\eta,\zeta;p)}{\partial\eta}\right|_{\eta=0} = 0, \quad \left.\frac{\partial\phi(\eta,\zeta;p)}{\partial\eta}\right|_{\eta=\infty} = 1,$$
$$\psi(0,\zeta;p) = 1, \quad \psi(\infty,\zeta;p) = 0$$

in which $p\in[0, 1]$ is an embedding parameter. When the parameter p increases from 0 to 1, the solution $f(\eta,\zeta;p)$ varies from $f_0(\eta)$ to $f(\eta)$ and the solution $\psi(\eta,\zeta;p)$ varies from $\theta_0(\eta)$ to $\theta(\eta)$. If these continuous variations are smooth enough, the Maclaurin's series with respect to p can be constructed for $\phi(\eta,\zeta;p)$ and $\psi(\eta,\zeta;p)$, respectively, and further, if these series are convergent at $p = 1$, we have:

$$f(\eta) = f_0(\eta) + \sum_{m=1}^{+\infty} f_m(\eta) = \sum_{m=0}^{+\infty}\phi_m(\eta,\zeta,\hbar_1) \tag{27}$$

$$\theta(\eta) = \theta_0(\eta) + \sum_{m=1}^{+\infty}\theta_m(\eta) = \sum_{m=0}^{+\infty}\psi_m(\eta,\zeta,\hbar_2) \tag{28}$$

where

$$f_m(\eta) = \frac{1}{m!}\left.\frac{\partial^m\phi(\eta,\zeta;p)}{\partial p^m}\right|_{p=0}, \quad \theta_m(\eta) = \frac{1}{m!}\left.\frac{\partial^m\psi(\eta,\zeta;p)}{\partial p^m}\right|_{p=0}$$

To calculate $f_m(\eta)$, we now differentiate eqs. (25) and (26) and related conditions m times with respect to p, then set $p = 0$, and finally divide by m!. The resulting m^{th}- order deformation problems are:

$$\mathrm{L}_1[f_m(\eta) - \chi_m f_{m-1}(\eta)] = \hbar_1 \mathrm{H}_1(\eta) R_{1,m}(\eta), \quad (m = 1, 2, 3, \ldots) \tag{29}$$

$$\mathrm{L}_2[\theta_m(\eta) - \chi_m \theta_{m-1}(\eta)] = \hbar_2 \mathrm{H}_2(\eta) R_{2,m}(\eta), \quad (m = 1, 2, 3, \ldots) \tag{30}$$

$$f_m(0) = 0, \quad f_m'(0) = 0, \quad f_m'(\infty) = 0, \quad \theta_m(0) = 0, \quad \theta_m(\infty) = 0 \tag{31}$$

where $R_{1,m}(\eta)$ and $R_{2,m}(\eta)$ are given by:

$$R_{1,m}(\eta) = (1+2\gamma\eta)f_{m-1}''' - 2\gamma f_{m-1}'' + \sum_{i=0}^{m-1}(f_i f_{m-i-1}'' - f_i' f_{m-i-1}') + \lambda\theta_{m-1} + (1-\chi_m)$$

$$R_{2,m}(\eta) = (1+2\gamma\eta)\theta_{m-1}'' + 2\gamma\theta_{m-1}' + \mathrm{Pr}\sum_{i=0}^{m-1}(f_i\theta_{m-i-1}' - \theta_i f_{m-i-1}')$$

where prime denotes differentiation with respect to η and:

$$\chi_m = \begin{cases} 0, & m \le 1, \\ 1, & m > 1 \end{cases}$$

The general solution of eqs. (29) and (30) are:

$$f_m(\eta) = \hat{f}_m(\eta) + C_1 + C_2\eta + C_3 e^{-\zeta\eta} \tag{32}$$

$$\theta_m(\eta) = \hat{\theta}_m(\eta) + C_4 + C_5 e^{-\zeta\eta} \tag{33}$$

where C_i for $i = 1, \ldots 5$ are constants, $\hat{f}_m(\eta)$ and $\hat{\theta}_m(\eta)$ are particular solutions of eqs. (29) and (30), respectively.

For simplicity, here we take $H_1(\eta) = H_2(\eta) = 1$. According to the rule of solution expression denoted by eqs. (14) and (15), $C_2 = C_4 = 0$. The other unknowns are governed by:

$$\hat{f}_m(0) + C_1 + C_3 = 0, \quad \hat{f}'_m(0) - \zeta C_3 = 0, \quad \hat{\theta}_m(0) + C_5 = 0$$

and according to our algorithm, the other boundary conditions are fulfilled. In this way, we derive $f_m(\eta)$ and $\theta_m(\eta)$ for $m = 1, 2, 3,...$, successively for every ζ.

At the N^{th}-order approximation, we have the analytic solution of eqs. (9) and (10), namely:

$$f(\eta) \approx F_N(\eta) = \sum_{i=0}^{N} f_i(\eta), \quad \theta(\eta) \approx\!= \Theta_N(\eta) = \sum_{i=0}^{N} \theta_i(\eta) \tag{34}$$

For simplicity, here we take $\hbar_1 = \hbar_2 = \hbar$. The auxiliary parameter $\hbar$ is useful to adjust the convergence region of the series (34) in the homotopy analysis solution. By plotting $\hbar$-curve, it is straightforward to choose an appropriate range for $\hbar$ which ensures the convergence of the solution series. As pointed out by Liao [11], the appropriate region for $\hbar$ is a horizontal line segment.

Rational bases

Invoking eqs. (9) and (10) and the boundary conditions (11), one can write:

$$f(\eta) = d_0 + \eta + \sum_{m=1}^{+\infty} \sum_{q=0}^{m-2} d_{q,m} \eta^q (1+\eta)^{-m} \tag{35}$$

$$\theta(\eta) = \sum_{m=1}^{+\infty} \sum_{q=0}^{m-2} e_{q,m} \eta^q (1+\eta)^{-m} \tag{36}$$

where d_0, $d_{q,m}$, and $e_{q,m}$ are coefficients to be determined. According to the rule of solution expression denoted by eqs. (35) and (36) and the boundary conditions (11), the initial approximations of $f(\eta)$ and $\theta(\eta)$ are selected as:

$$f_0(\eta) = f_0 - 1 + \eta + \frac{1}{1+\eta} \tag{37}$$

$$\theta_0(\eta) = \frac{1}{1+\eta} \tag{38}$$

The auxiliary linear operators L_1 and L_2 are :

$$L_1[\phi(\eta; p)] = \left(\frac{\partial^3}{\partial \eta^3} + \frac{3}{1+\eta} \frac{\partial^2}{\partial \eta^2} \right) \phi(\eta; p) \tag{39}$$

$$L_2[\psi(\eta; p)] = \left(\frac{\partial^2}{\partial \eta^2} + \frac{2}{1+\eta} \frac{\partial}{\partial \eta} \right) \psi(\eta; p) \tag{40}$$

$$L_1[D_1 + D_2\eta + D_3(1+\eta)^{-1}] = 0, \quad L_2[D_4 + D_5(1+\eta)^{-1}] = 0 \tag{41}$$

where D_i, $i = 1, 2, ..., 5$ are constants. This choice of L_1 and L_2 is motivated by eqs. (35) and (36), respectively, and from boundary conditions (11), we have $D_2 = D_4 = 0$.

In this case, the non-linear operator $N_i[\phi, \psi]$, the homotopy $H_i[\phi, \psi]$, $R_{i,m}(\eta)$ for $i = 1$, 2, and the zero-order deformation equations, the m^{th}-order deformation equations are designed as in the previous case without the parameter ζ.

The general solution of m^{th}-order deformation equations here are:

$$f_m(\eta) = \hat{f}_m(\eta) + D_1 + D_2\eta + D_3(1+\eta)^{-1} \tag{42}$$

$$\theta_m(\eta) = \hat{\theta}_m(\eta) + D_4 + D_5(1+\eta)^{-1} \tag{43}$$

where D_i for $i = 1, \ldots, 5$ are constants, $\hat{f}_m(\eta)$ and $\hat{\theta}_m(\eta)$ are particular solutions of m^{th}-order deformation equations.

By rule of solution expressions denoted by (35) and (36) and from m^{th}-order deformation equations, the auxiliary functions $H_1(\eta)$ and $H_2(\eta)$ are chosen in the form:

$$H_1(\eta) = (1+\eta)^{-\xi_1}, \quad H_2(\eta) = (1+\eta)^{-\xi_2}$$

It is found that when $\xi_1 < 4$ and $\xi_2 < 3$ the term $\log(1+\eta)$ appears in the solution expression of $f_m(\eta)$ and $\theta_m(\eta)$, which disobeys the rule of solution expression denoted by (35) and (36), respectively. In addition, when $\xi_1 > 4$ and $\xi_2 > 3$ we omit some terms in solution expression. This uniquely determines the corresponding auxiliary functions:

$$H_1(\eta) = (1+\eta)^{-4}, \quad H_2(\eta) = (1+\eta)^{-3}$$

According to (35) and (36), $D_2 = D_4 = 0$. The other unknowns are governed by:

$$\hat{f}_m(0) + D_1 + D_3 = 0, \quad \hat{f}'_m(0) - D_3 = 0, \quad \hat{\theta}_m(0) + D_5 = 0$$

and according to our algorithm, the other boundary conditions are satisfied. In this way, we derive $f_m(\eta)$ and $\theta_m(\eta)$ for $m = 1, 2, 3, \ldots$, successively. Like previous case, we will take here $\hbar_1 = \hbar_2 = \hbar$.

Numerical results and discussion

We use the widely applied symbolic computation software MATHEMATICA to solve eqs. (29) and (30). By means of the so-called $\hbar$-curve, it is straightforward to choose an appropriate range for $\hbar$ which ensures the convergence of the solution series. As pointed out by Liao [11], the appropriate region for $\hbar$ is a horizontal line segment. We can investigate the influence of $\hbar$ on the convergence of $f''(0)$ and $-\theta'(0)$, by plotting the curve of it *vs.* $\hbar$, as shown in figs. 1-4 (for $\lambda > 0$) and figs. 5-8 (for $\lambda < 0$) are the examples of two cases. By considering the $\hbar$-curve we can obtain the reasonable interval for $\hbar$ in each case. Our computations show that in first case it is better to we choose $\zeta \geq 2$.

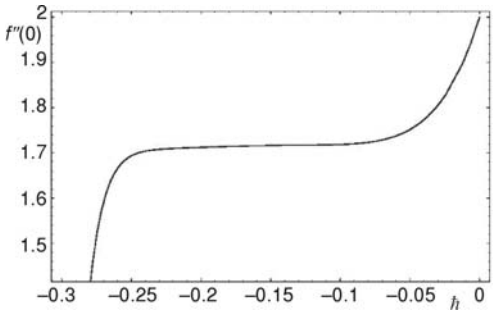

Figure 1. The $\hbar$-curve of the $f''(0)$ *vs.* $\hbar$ for the 20^{th}-order approximation and Pr = 0.7, $\zeta = 2$, $\gamma = 0$, $\lambda = 1$, and $f_0 = 0$ by exponential bases

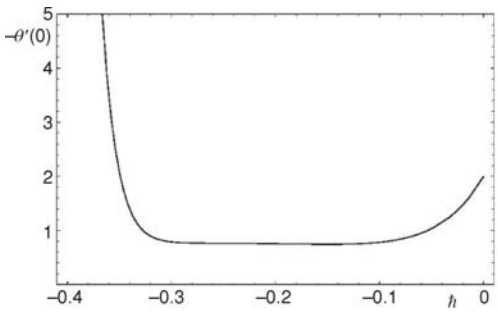

Figure 2. The $\hbar$-curve of the $-\theta'(0)$ *vs.* $\hbar$ for the 20^{th}-order approximation and Pr = 0.7, $\zeta = 2$, $\gamma = 0$, $\lambda = 1$, nd $f_0 = 0$ by exponential bases

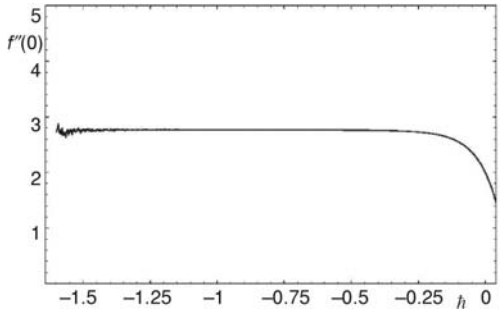

Figure 3. The $\hbar$-curve of the $f''(0)$ *vs.* $\hbar$ for the 20th-order approximation and Pr = 0.7, $\gamma = 1$, $\lambda = 1$, and $f_0 = 0$ by rational bases

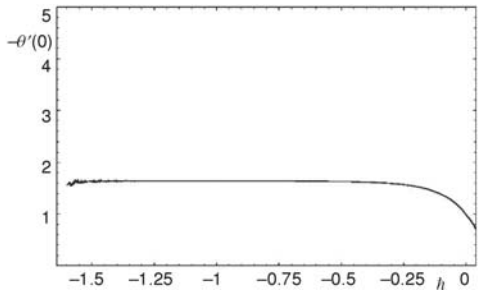

Figure 4. The $\hbar$-curve of the $-\theta'(0)$ *vs.* $\hbar$ for the 20th-order approximation and Pr = 0.7, $\gamma = 1$, $\lambda = 1$, and $f_0 = 0$ by rational bases

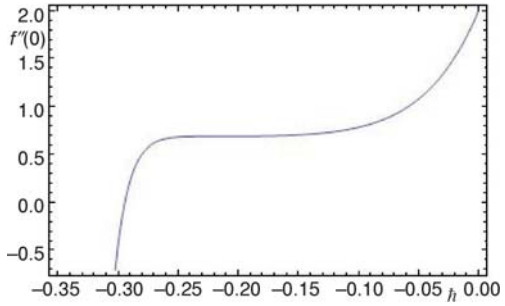

Figure 5. The $\hbar$-curve of the $f''(0)$ *vs.* $\hbar$ for the 20th-order approximation and Pr = 0.7, $\zeta = 0$ $\gamma = 0$, $\lambda = -1$, and $f_0 = 0$ by exponential bases

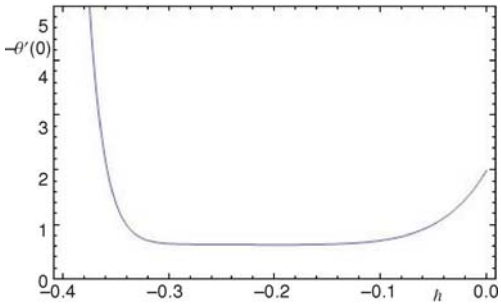

Figure 6. The $\hbar$-curve of the $-\theta'(0)$ *vs.* $\hbar$ for the 20th-order approximation and Pr = 0.7, $\zeta = 2$ $\gamma = 0$, $\lambda = -1$, and $f_0 = 0$ by exponential bases

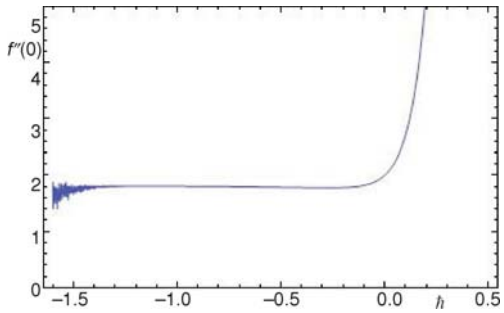

Figure 7. The $\hbar$-curve of the $f''(0)$ *vs.* $\hbar$ for the 20th-order approximation and Pr = 0.7, $\gamma = 1$, $\lambda = -1$, and $f_0 = 0$ by rational bases

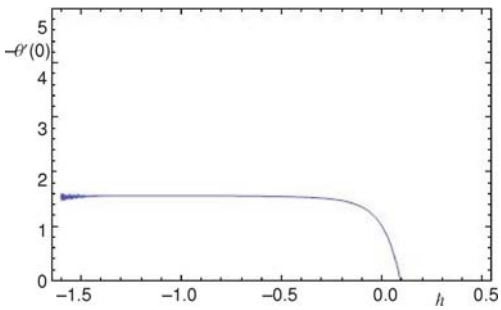

Figure 8. The $\hbar$-curve of the $-\theta'(0)$ *vs.* $\hbar$ for the 20th-order approximation and Pr = 0.7, $\gamma = 1$, $\lambda = -1$, and $f_0 = 1$ by rational bases

Also, by computing the error of norm 2 for two successive approximation of $F_N(\eta)$ or $\Theta_N(\eta)$ of (34), we can obtain the best value for $\hbar$ in each case. Figures 9 and 10 show the error of $F_{20}(\eta)$ for $\eta \in [0, 5]$ in first case and we obtain that the best value of $\hbar$ is –0.209 with error

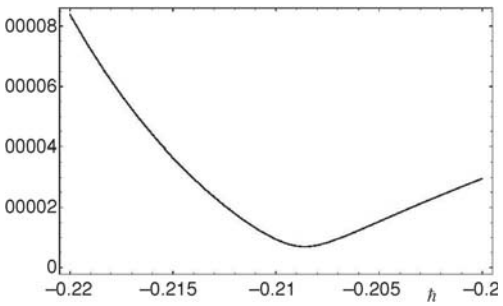

Figure 9. The norm 2 error of $F_{20}(\eta)$ *vs.* $\hbar$ with Pr = 0.7, $\zeta = 2$ $\gamma = 0$, $\lambda = 1$, and $f_0 = 0$ by exponential bases

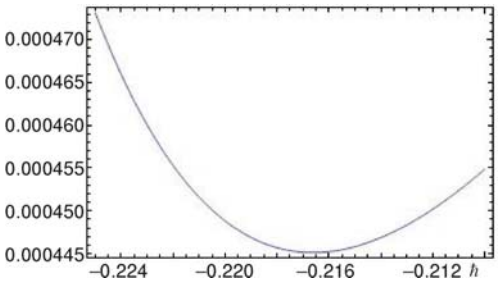

Figure 10. The norm 2 error of $F_{20}(\eta)$ *vs.* $\hbar$ with Pr = 0.7, $\zeta = 2$ $\gamma = 0$, $\lambda = -1$, and $f_0 = 0$ by exponential bases

$7.02 \cdot 10^{-6}$ (for $\lambda > 0$) and $\hbar$ is –0.218 with error $6.02 \cdot 10^{-5}$ (for $\lambda < 0$), respectively. With the same contrast figs. 11 and 12 show the error of $\Theta_{20}(\eta)$ in second case and we obtain that the best value of $\hbar$ are –1.327 and –1.95 with error $3.47 \cdot 10^{-7}$ and $3.18 \cdot 10^{-8}$ for $\lambda < 0$ and $\lambda > 0$, respectively.

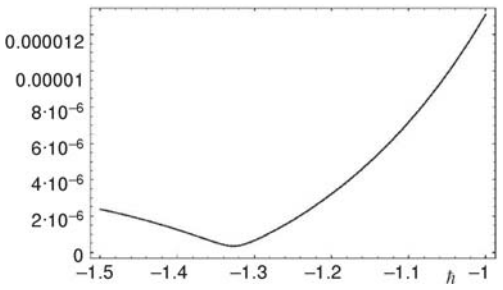

Figure 11. The norm 2 error of $\Theta_{20}(\eta)$ *vs.* $\hbar$ with Pr = 0.7, $\gamma = 1$, and $\lambda = 1$, $f_0 = 0$ by rational bases

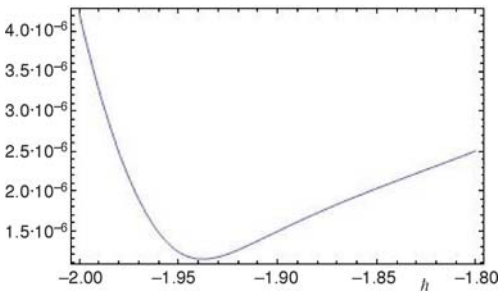

Figure 12. The norm 2 error of $\Theta_{20}(\eta)$ *vs.* $\hbar$ with Pr = 0.7, $\gamma = 1$, $\lambda = -1$, and $f_0 = 0$ by rational bases

The so-called homotopy-Pade technique (see [11]) is employed, which greatly accelerates the convergence. The [r, s] homotopy-Pade approximations of $f''(0)$ (or C_f), and $-\theta'(0)$ (or Nu_x) in eq. (13), according to eqs. (27) and (28) are formulated by:

$$\frac{\sum_{k=0}^{r} \phi_k''(0,\hbar)}{1+\sum_{k=1}^{s} \phi_{n+k+1}''(0,\hbar)}, \quad \frac{-\sum_{k=0}^{r} \psi\phi_k'(0,\hbar)}{1-\sum_{k=1}^{s} \psi'_{n+k+1}(0,\hbar)}$$

respectively. In many cases, the [*r*, *r*] homotopy-Pade approximation does not depend upon the auxiliary parameter $\hbar$. To verify the accuracy of HAM, comparisons of $f''(0)$ and $-\theta'(0)$ with those reported by Ramachandran *et al*. [23], Hassanien and Gorla [24], Lok *et al*. [25], and Ishak *et al.* [10] (upper branch values) are given in tabs. 1 and 2 for $\lambda = 1$ and tabs. 3 and 4 for $\lambda = -1$ when $f_0 = \gamma = 0$ and different values of Pr, respectively.

Table 1. Results for [*15, 15*] homotopy-Pade approach for $f''(0)$ for exponential bases when $\lambda > 0$

Pr	Ramachandran *et al.* [23]	Hassanien and Gorla [24]	Lok *et al*. [25]	Ishak *et al.* [26]	HAM	
					Case 1	Case 2
0.7	1.7063	1.70632	1.7064	1.7063	1.70633	1.70632
1	–	–	–	1.6754	1.67543	1.67547
7	1.5179	–	1.5180	1.5179	1.51504	1.51787
10	–	1.49284	–	1.4928	1.48361	1.49281
20	1.4485	–	1.4486	1.4485	1.41955	1.44847
40	1.4101	–	1.4102	1.4101	1.34401	1.41376
50	–	1.40686	–	1.3989	1.31251	1.40384
60	1.3903	–	1.3903	1.3903	1.28181	1.38853
80	1.3774	–	1.3773	1.3774	1.21908	1.37220
100	1.3680	1.38471	1.3677	1.3680	1.15091	1.36176

Table 2. Results for [*15, 15*] homotopy-Pade approach for $-\theta'(0)$ for rational bases when $\lambda > 0$

Pr	Ramachandran *et al.* [23]	Hassanien and Gorla [24]	Lok *et al*. [25]	Ishak *et al.* [26]	HAM	
					Case 1	Case 2
0.7	0.7641	0.76406	0.7641	0.7641	0.76406	0.76406
1	–	–	–	0.8708	0.87079	0.87074
7	1.7224	–	1.7226	1.7224	1.71284	1.72236
10	–	1.94461	–	1.9446	1.90718	1.94462
20	2.4576	–	2.4577	2.4576	2.83443	2.46210
40	3.1011	–	3.1023	3.1011	3.34308	3.09395
50	–	3.34882	–	3.3415	3.56039	3.33583
60	3.5514	–	3.5560	3.5514	3.73733	3.54544
80	3.9095	–	3.9195	3.9095	4.00633	3.90255
100	4.2116	4.23372	4.2289	4.2116	4.20065	4.19654

Table 3. Results for [*15, 15*] homotopy-Pade approach for $f''(0)$ and $-\theta'(0)$ for exponential bases when $\lambda < 0$

Pr	$f''(0)$	$-\theta'(0)$	Pr	$f''(0)$	$-\theta'(0)$
0.7	0.69166	0.63325	40	1.03355	3.28208
1	0.73141	0.73141	50	1.05328	3.50010
7	0.93929	1.53467	60	1.07171	3.67989
10	0.92896	1.71625	80	1.10605	3.95540
20	0.98383	2.94287	100	1.13784	4.15545

Table 4. Results for [*15, 15*] homotopy-Pade approach for $f''(0)$ and $-\theta'(0)$ for rational bases when $\lambda < 0$

Pr	$f''(0)$	$-\theta'(0)$	Pr	$f''(0)$	$-\theta'(0)$
0.7	0.69149	0.63319	40	1.04527	2.89948
1	0.73124	0.73132	50	1.04887	3.13856
7	0.92339	1.54611	60	1.06128	3.34669
10	0.95258	1.76342	80	1.07903	3.70261
20	1.00325	2.26820	100	1.08650	4.00749

Conclusions

Here we have applied the homotopy analysis method which has been proven to be successful in tackling non-linear problems to compute the influence of suction/injection on the mixed convection flows along a vertical cylinder. It is interesting to note that when $\gamma = 0$ then one recovers the flat plate case [26]. The problem reduces to the case of impermeable cylinder for $f_0 = 0$ [27]. The case of arbitrary surface temperature can also be recovered by $\gamma = f_0 = 0$ [23]. It is further revealed that usage of rational base is easier, because it has one auxiliary parameter less than the exponential case (ζ). It is worth mentioning that in both cases, the dual solutions do not obtain, therefore, the comparison with existing results reveal that our series solutions are valid for all values λ.

Acknowledgments

R. Ellahi thanks to United State Education Foundation Pakistan and CIES USA to honored him by Fulbright Scholar Award for the year 2011-2012. RE and A. Riaz are also grateful to the Higher Education Commission for NRPU and financial support.

Nomenclature

k – thermal conductivity, [$Wm^{-1}K^{-1}$]
Nu_x – Nusselt number, [–]
Re_x – local Reynolds number, [–]
T – fluid temperature, [K]
T_w – surface temperature, [K]
T_∞ – ambient temperature, [K]
U_∞ – free stream velocity, Ls^{-1}]
u, w – velocity components, [ms^{-1}]
x, y – cartesian components, [l]

Greek symbols

α – thermal diffusivity, [m^2s^{-1}]
η – similarity variable, [m]
θ – dimensionless temperature, [–]
μ – dynamic viscosity, [Nsm^{-2}]
ν – kinematics viscosity, [m^2s^{-1}]
ρ – fluid density, [kgm^{-3}]
ψ – stream function, m^2s^{-1}]

References

[1] Vafai, K., *Handbook of Porous Media*, 2nd ed., Taylor & Francis, New York, N. Y., USA, 2005
[2] Vafai, K., *Porous Media: Applications in Biological Systems and Biotechnology*, Taylor & Francis, New York, N. Y., USA, 2010
[3] Tan, W. C., Masuoka, T., Stokes' First Problem for a Second Grade Fluid in a Porous Half Space with Heated Boundary, *Int. J. Nonlinear Mech,. 40* (2005), 4, pp. 512-522
[4] Tan, W. C., Masuoka, T., Stability Analysis of a Maxwell Fluid in a Porous Medium Heated From Below, *Phys. Lett. A, 360* (2007), 3, pp. 454-460
[5] Fetecau, C., Hayat, T., MHD Transient Flows in a Channel of Rectangular Cross-Section with Porous Medium, *Physics letters A, 369* (2007), 1-2, pp. 44-54

[6] Hayat, T., *et al*., Unsteady Solutions in a Third-Grade Fluid Filling the Porous Space, *Mathematical Problems in Engineering, 2008* (2008), ID 139560
[7] Pop, I., Ingham, D. B., *Convective Heat Transfer*, Pergamon, Amsterdam, The Netherlands, 2001
[8] Mahmood, T., Merkin, J. H., Similarity Solutions in Axisymmetric Mixed Convection Boundary-Layer Flow, *J. Eng. Math., 22* (1988), 1, pp. 73-92
[9] Ridha, A., Aiding Flows Non-Unique Similarity Solutions of Mixed Convection Boundary-Layer Equations, *Z. Angew. Math. Pys. (ZAMP), 47* (1996), 3, pp. 341-352
[10] Ishak, A., *et al*., The Effects of Transpiration on the Boundary Layer Flow and Heat Transfer over a Vertical Slender Cylinder, *Int. J. Non-Linear Mech., 42* (2007), 8, pp. 1010-1017
[11] Liao, S. J., *Beyond Perturbation: Introduction to the Homotopy Analysis Method*, CRC Press, Chapman & Hall, Boca Raton, Fla., USA, 2003
[12] Xu, H., *et al*., Series Solutions of Unsteady Boundary Layer Flow of a Micropolar Fluid Near the Forward Stagnation Point of a Plane Surface, *Acta Mech., 184* (2006), 1, pp. 87-101
[13] Cheng, J., Series Solutions of Nano Boundary Layer Flows by Means of the Homotopy Analysis Method, *J. Math. Anal. Appl., 343* (2008), 1, pp. 233-245
[14] Abbasbandy, S., Homotopy Analysis Method for Generalized Benjamin-Bona-Mahony Equation, *Z. Angew. Math. Phys. (ZAMP) 59* (2008), 1, pp. 51-62
[15] Xu, H., *et al*., Series Solutions of Unsteady Free Convection Flow in the Stagnation-Point Region of a Three-Dimensional Body, *Int. J. Therm. Sci., 47* (2008), 5, pp. 600-608
[16] Ellahi, R., Zeeshan, A., A Study of Pressure Distribution of a Slider Bearing Lubricated with Second Grade Fluid, *Numerical Methods for Partial Differential Equations, 27* (2011), 5, pp. 1231-1241
[17] Liao, S. J., A General Approach to Get Series Solution of Non-Similarity Boundary-Layer Flows, *Commun. Nonlinear Sci. Numer. Simulat., 14* (2009), 5, pp. 2144-2159
[18] Ellahi, R., Effects of the Slip Boundary Condition on Non-Newtonian Flows in a Channel, *Communication in Nonlinear Science and Numerical Simulations, 14* (2009), 4, pp. 1377-1384
[19] Gebhart, B., *et al.*, *Buoyancy Induced Flows and Transport*, Hemisphere, New York, USA, 1988
[20] Rajagopal, K. R., *et al*., On the Oberbeck-Boussinesq Approximation, *Math. Models Methods Appl. Sci. 6* (1996), 8, pp. 1157-1167
[21] Van Gorder, R. A., Vajravelu, K., On the Selection of Auxiliary Functions, Operators, and Convergence Control Parameters in the Application of the Homotopy Analysis Method to Nonlinear Differential Equations: A General Approach, *Commun. Nonlinear Sci. Numer. Simul., 14* (2009), 12, pp. 4078-4089
[22] Liao, S. J., Notes on the Homotopy Analysis: Some Definitions and Theorems, *Commun. Nonlinear Sci. Numer. Simulat., 14* (2009), 4, pp. 983-997
[23] Ramachandran, N., *et al*., Mixed Convection in Stagnation Flows Adjacent to a Vertical Surface, *ASME J. Heat Transfer, 110* (1988), 2, pp. 373-377
[24] Hassanien, I. A., Gorla, R. S., Combined Forced and Free Convection in Stagnation Flows of Micropolar Fluids Over Vertical Non-Isothermal Surface, *Int. J. Eng. Sci., 28* (1990), 8, pp. 783-792
[25] Lok, Y. Y., *et al.*, Unsteady Mixed Convection Flow of a Micropolar Fluid Near the Stagnation Point on a Vertical Surface, *Int. J. Therm. Sci., 45* (2006), 12, pp. 1149-1157
[26] Ishak, A., *et al*., Dual Solutions in Mixed Convection Flow Near a Stagnation Point on a Vertical Porous Plate, *Int. J. Thermal Sci., 47* (2008), 4, pp. 417-422
[27] Mahmood, T., Merkin, J. H., Similarity Solutions in Axisymmetric Mixed-Convection Boundary-Layer Flow, *J. Eng. Math., 22* (1988), 1, pp. 73-92

Paper submitted: September 23, 2012
Paper revised: April 26, 2013
Paper accepted: April 27, 2013